Sustainable thermochemical single-step process to obtain Magnetic Activated Carbons from chestnut industrial wastes

*S. Rodríguez-Sánchez †, B. Ruiz †, D. Martínez-Blanco ‡, M. Sánchez-Arenillas§, I. Suárez-Ruiz †, M.A. Diez †, J. F. Marco§, J. A. Blanco ″, E. Fuente†**

†Biocarbon & Sustainability Group. Instituto Nacional del Carbón (INCAR), CSIC, 33011, Oviedo, Spain.

‡ Scientific-Technical Services, University of Oviedo, 33006, Oviedo, Spain.

§ Instituto de Química-Física "Rocasolano", CSIC, Serrano 119, 28006 Madrid, Spain

″Department of Physics, University of Oviedo, 33007 Oviedo Spain.

ABSTRACT

A novel thermochemical process based on a single step was optimized to obtain activated carbons with magnetic and/or catalytic properties from an industrial biomass waste. Anhydrous iron chloride was used as an activating agent and mixed directly with the chestnut shell waste. To study the effect of the activation temperature and its influence in the magnetic properties of the materials, a series of samples obtained in a range between 220-800ºC were studied. The results demonstrated the presence of different iron compounds depending on the activation temperature set, as well as their influence on morphological and textural development of the magnetic activated carbons (BET specific surface area, S_{BET}, up to 568 m^2/g, total pore volume, V_{TOT}, up to 0.294 cm^3/g *versus* to 1 m^2/g and 0.007 cm^3/g, respectively, for the raw biomass waste). The analyses and techniques employed, especially specific techniques as Mössbauer spectroscopy showed relative contributions of the different iron phases in the materials (magnetite, maghemite, metallic iron…) being the most complex Fe-distribution in the activated carbon obtained at 800ºC. Additionally, the magnetic properties measured by Vibrating Sample Magnetometer, VSM, confirmed the coexistence of different ferromagnetic phases being the remanent magnetization, M_R, (up to 3.88 emu/g) and coercivity, H_c, (up to 140 Oe), larger as activation temperature increases. In general, the high temperature favoured the development and evolution towards other related iron compounds, while at low temperature, 220ºC, the presence of these compounds were null and their behaviour resembling the results obtained for the original biomass waste.

KEYWORDS: Biomass, Chestnut industrial waste, Food industry, Magnetic activated carbon (MAC), Sustainable activation, One-step chemical activation, Vibrating Sample Magnetometer (VSM)

▪ INTRODUCTION

In recent years, environmental contamination in air, soil and water has become a serious problem and the introduction of stricter environmental regulations promotes the search for solutions developing new techniques and materials to face them. An alternative increasingly demanded materials are activated carbons (ACs), due to their appropriate characteristics as adsorbents to remove pollutants[1].

The preparation of this kind of materials can be done from very diverse precursors, the most used are wood, peat and coals, although during the last years those obtained from biomass wastes have been investigated more frequently with good and promising results[2-7].

The production of ACs from biomass wastes result into a low-cost materials and friendly to the environment to retain mercury[5], to remove volatile organic compounds (VOCs)[3] or for the wastewater treatment to remove hazardous pollutants such as heavy metals, dyes[2, 7] and pharmaceutical and personal care products (PPCPs) and others as phenolic compounds[7]**.** Activated carbons from biomass wastes can be also highly suitable for CO_2 capture[6] due the gas storage capacities of the biomass based activated carbons[2]**.**

Search for novel sources to produce ecofriendly low-cost activated carbons and their multiple environmental applications as well as the increasing interest in the improvement of their characteristics and effectiveness as adsorbents and catalytic supports have resulted in the obtaining of Magnetic Activated Carbons (MACs)[8-12], a class of carbonaceous materials with an undeniable adsorption capacity and magnetic properties. Currently, the use of natural precursors such as biomass wastes is an emerging and important low-cost sustainable alternative and natural precursor [10, 13] to make MACs. Recent studies show that this type of MACs are very suitable materials for multiple applications, e.g. CO_2 adsorption[11 12]; wastewater [7, 14]**;** medical applications[9, 15]**;** catalysts[12, 16].

The transformation of an activated carbon into magnetic derivatives is being studied using various methods for its preparation[15, 17]: chemical precipitation[18-19]**,** high temperature treatment[20-21]; or encapsulation[22]. On the other hand, a MAC can be developed from a biomass through a chemical activation process with a previous pyrolysis step of the precursor[23] or without it[10, 14]. In these cases, the precursor (biomass or pyrolyzed biomass) gets in touch with the activating agent (iron salt) usually by impregnation[10, 14], and then the activation process is carried out.

The biomass wastes usually employed are from different origins and nature[10, 14, 16, 23]. This work is focused on chestnut shell wastes (CH) due its suitable characteristics [24], important industrial waste role and barely studied in this field.

Chestnut is the fruit of the chestnut tree, Castanea Sativa. Nowadays, world chestnut production is estimated on 2 Mt[25], while in 60's years of XX Century it was around 600 kt. The production is based in two main regions: Europe and Asia, although there are other emerging countries producers (Australia, Chile or USA). In Europe is mainly produced in the south part of the continent but Turkey is the biggest European producer with 60 kt[26]. Likewise, there is a well-developed agro-food industry in Europe that needs a constantly quantity of chestnuts to support their fresh consumption and transformation: marron glacé, candied products, etc.[27] Despite this, few studies are involved in CH and their applications as activated carbons[24, 28] and it is practically null in terms of MACs, although recently, at Esra Altintig et al.work[29], bio-based magnetic activated carbon from this waste resulted as a potential sorbents for effective removal of malachite green from wastewaters.

The present work introduces several novel aspects in MACs preparation that have not been studied in other works with any biomass before. The contact, between the CH and the activating agent will not be carried out by impregnation (more usual method), but by physical mixture. On the other hand, an only one-step thermochemical activation process turning it much more optimal, sustainable and economical.

In this research work, considering a scenario of circular economy, is raised to advance in the use of industrial biomass wastes by transforming them into carbonaceous adsorbent materials with magnetic and or catalytic properties. The specific challenges are focused on the optimization of the experimental conditions for the chemical activation process and the effects on the development of chemical, morphological, textural and magnetic properties in magnetic activated carbons (MACs). In general, the major goal of this study is to develop an experimental methodology of novel chemical activation that allows the management and sustainable valorization of a raw biomass industrial waste and its transformation into MACs.

▪ EXPERIMENTAL SECTION

Industrial biomass waste. A chestnut Shell waste (CH) was used as raw material in the preparation of Magnetic Activation Carbons (MACs). CH is an industrial food-waste generated from the peeling process in the preparation of candied products (i.e. marron-glacé, chestnut jam, etc…). It was supplied by an industry located in El Bierzo-León, in the north of Spain.

CH waste was grounded and crushed to a fine particle size (< 3mm) to favor the physical mixing with the activating agent and the process of chemical activation.

Preparation of Magnetic Activated Carbons (MACs). Magnetic activated carbons were obtained using a novel single-step thermochemical process based on the direct physical mixture of the raw CH and the anhydrous FeCl used as the activating agent. The proposed single-step process differs from the employed by other authors[8, 10, 30] in two aspects: the activating agent used for carbon activation is the anhydrous iron salt versus the hydrated iron salt, and the no requirement of an impregnation of the carbon source with the chemical activation agent.

The activating agent and the crushed biomass waste were mixed in solid state chemical in a weight ratio 0.5:1. The chemical activation process was carried out in a conventional tubular furnace, Carbolite CTF 12/65//550, at a heating rate of 5ºC min^{-1} from ambient to six different final temperatures: 220, 400, 500, 600, 700 and 800 °C and the desired final temperature was maintained for 60 min under a constant N_2 flow rate of 150 ml/min. These variables were selected on the basis of previous studies in our research group[3, 6, 24].

After thermochemical process, MACs were washed to remove products that could be blocking the porosity. Samples were repetitively washed with deionized water (Milli-Q) and finally, they were dried at 105ºC and then in a vacuum stove at 60ºC.

Characterization of the materials. The chemical characterization of the samples consisted of moisture and ash determination and elemental composition. The moisture of the sample was obtained following the UNE 33002 standard, on the basis of the weight loss at 105ºC over a period of 1 h. The ash content was determined by calcination at 815ºC for 1 h in presence of oxygen, according to the UNE 32004 standard procedure.. The elemental analysis was carried out using a LECO CHN-2000 for C, H and N (ASTM D-5773) and a LECO S-144 DR (ASTM D-5016) for sulphur.

The inorganic composition of CH, was determined by inductively coupled plasma and mass spectrometry (ICP-MS). For this analysis the chestnut shell ashes were digested in a microwave oven with a mixture of nitric and hydrochloric acids. An Agilent 7700x ICP-MS equipment was used for the elemental analysis.

X-ray diffraction (XRD) measurements were carried out in a Bruker D8 Advance diffractometer equipped with a graphite monochromator and an internal silicon powder pattern was used as reference material. The equipment was connected to a CuKα radiation source. The diffraction data were collected by step scanning using a step size of 0.02° and a step-time of 3 s. The scan range 2θ was from 5º to 80º.

Fourier-Transform infrared (FTIR) spectra were collected on a Nicolet IR 8700 spectrophotometer fitted with a deuterated triglycerine sulphate (DTGS) detector. All spectra were obtained in the mid-IR region, 4000-400 cm^{-1}, in the transmission mode by co-adding 128 scans at a resolution of 4 cm^{-1}. The spectra were recorded using KBr standard pellets.

Raman spectroscopy analysis was performed to compliment the results from FTIR. The Raman spectra were obtained using a JYV-Jobin Yvon spectrometer LabRam HR UV 800 model with an Olympus confocal microscope BXFM-ILHS using DPSS laser model CDPS532M: 532 nm diode laser. CCD detector and working conditions: grating 950 l / mm, objective x100, hole 200, spectral interval analyzed (120-1850 cm^{-1} and 120-800 cm^{-1}), 4 accumulations / 35 sg each and calibration with silicon plate at 520.80 cm^{-1}.

Mössbauer spectra were recorded at room temperature (RT) in the transmission mode using a constant acceleration spectrometer equipped with a $^{57}Co(Rh)$ source. The samples were prepared to give an effective absorber thickness of 5 mg of natural iron per cm^2. The velocity scale was calibrated using a 6 μm thick α-iron foil and the isomer shifts were referred to the centroid of the spectrum of α-iron at RT. The spectra were computer-fitted using the usual constraints of equal area and width for the two lines of a doublet and equal width and areas in the ratio 3:2:1:1:2:3 for the six lines of a doublet. The relative concentrations of each iron species were obtained from their relative areas assuming equal recoil-free fractions at RT for all the spectral components.

The morphological properties of the MACs were examined using a scanning electron microscope (ZEISS Model DMS-942) equipped with an energy-dispersive X-ray analysis system (Link-Isis II), SEM-EDX. To decrease the charging of the samples and to improve the SEM pictures the samples were covered with iridium prior to SEM examination.

The true density of MACs was obtained by helium picnometry on a Micromeritics AccuPyc 1330 pycnometer. The textural properties of the materials were characterized from N_2 adsorption isotherms at 77K in a Micrometics ASAP 2420 system and CO_2 adsorption isotherms at 273 K on a Quantachrome NOVA 4000 model instrument.

Before helium picnometry, N_2 and CO_2 adsorption, the samples were outgassed under vacuum at 393 K overnight to remove any adsorbed moisture and/or gases.

A vibrating sample magnetometer, VSM, (Microsense EV-9) was used to measure magnetic properties by means of the M(H) magnetization hysteresis curve in the field range from -20 to 20 kOe at RT. In order to perform measurements, about 50 mg of every powder sample were compacted and encapsulated into a 70 mm^3 acrylic cup which is firmly stuck to an 8 mm Pyrex transverse rod by means double side Scotch® tape.

▪ RESULTS AND DISCUSSION

Chemical Characterization. **Table 1** shows the ultimate analysis of the CH and MACs together with the ash and iron contents. The final pHs of the MACs after washing several times with deionized water (Milli-Q) until a stable value of pH was reached, are also presented in **Table 1**.

Information about the molecular structure reveals that the carbon percentage (50.27%, db) associated with low ash and sulphur values maked CH as a suitable precursor of MACs. Such key characteristics are preferred in the production of ACs[3, 6, 31]. It is also important to point out that the chemical composition of chestnut shells depend on the variety and where they come from. However, the chemical composition of the CH in this study is consistent with the wastes used by other authors to obtain ACs[24, 32].

The activation temperature has a remarkable influence in the chemical composition of the MACs, **Table 1.** These materials have high carbon content (67-70%, db), except in the sample at the lowest temperature of 220ºC (58.9%, db), although this content is always superior to that presented in the CH sample (50.27 %,db). The hydrogen content varies from 5.30% in CH to as low as 0.98% for the MAC at the highest temperature. Minor elements, S and N, in the raw CH do not follow a general pattern in the MACs. The results of the iron content present in MACs, as determined by ICP-MS, increases progressively with an increase in the activation temperature from 0.55 % in CH, only 1.06% in MAC obtained at 220ºC and finally up to 23.46 % in MAC obtained at 800°C. A similar trend was found in the MAC prepared from the lignin hydrochar derived from eucalyptus at 700ºC and 800ºC[11]. The amount of ashes also increases with the activation temperature in these materials (up to 34.5% in sample at 800ºC versus 0.9% in the raw material biowaste) due to the iron incorporation into the MACs.

Usually, the resulting material after a chemical activation was washed using HCl and repetitive washes with deionized water (Milli-Q), to eliminate the traces of activating agent and other products that could be blocked the porosity of the material obtained. In this work the materials obtained were washed exclusively with water because the hydrolysis of certain species of iron already generate the acidity in the wash. With this procedure, the process of obtaining MACs becomes more sustainable.

Table 1. Ash content and chemical composition of the precursor (CH) and the magnetic activated carbons (MACs) at different temperatures.

Nomenclature	**T(ºC)**	**Mass fraction (%) db**							
		Ash	**C**	**H**	**N**	**S**	**O[a]**	**Fe**	**pH**
CH		0.87	50.27	5.30	0.52	0.02	46.54	0.55	---
CH-A220H0.5-w	**220**	2.00	58.90	3.59	0.48	---	35.97	1.06	4.0
CH-A400H0.5-w	**400**	12.94	67.84	2.46	0.55	0.13	19.57	9.45	2.3
CH-A500H0.5-w	**500**	16.00	66.86	2.69	0.81	0.08	20.76	8.80	2.8
CH-A600H0.5-w	**600**	22.00	70.38	2.05	0.90	0.05	15.45	11.17	3.0
CH-A700H0.5-w	**700**	25.25	68.44	1.48	0.83	0.04	12.52	16.69	3.5
CH-A800H0.5-w	**800**	34.50	67.82	0.98	0.93	----	6.81	23.46	5.2

[a]The oxygen content was determined by difference.

Fig. 1 represents the XRD diffractograms corresponding to CH and MACs obtained at different temperatures. In the raw material (CH) and in the sample activated at the lowest temperate of 220ºC (CH-A220) only broad humps between 10 to 30º at 2θ are observed in these two samples which could be assigned to the amorphous carbon[29]. However the patterns of samples obtained at activation temperature equal or greater than 400ºC show well-resolved peaks at 2θ values around 18.32°, 30.13°, 35.49°, 37.07º, 43.10°, 53.49°, 57.01º and 62.60°. These Bragg peaks are indexed to (111), (220), (311), (222), (400), (422), (511) and (440) reflections of magnetite, Fe_3O_4, with a face-centered cubic (fcc) structure (PDF-2 card no. 01-08-0691). Besides that, a low-intensity peak at 2θ=44.71º is also found, and it is very likely to be related to the most intensity reflection (110) of metallic iron, Fe[52] (PDF-2 card no. 01-09-7194).

These peaks are similar to those found by other authors who have used different precursors and methodologies in the obtention of MACs[23, 29-30, 33-35], where the formation of crystalline magnetite was also confirmed by XRD. Moreover, in Shengli Zhang et al. research the effect of high activation temperature (above 650ºC) on the MACs led to crystal structure transformation of Fe_3O_4 to produce well-crystallized Fe and at 700-800ºC several Fe_3C peaks appeared[23].

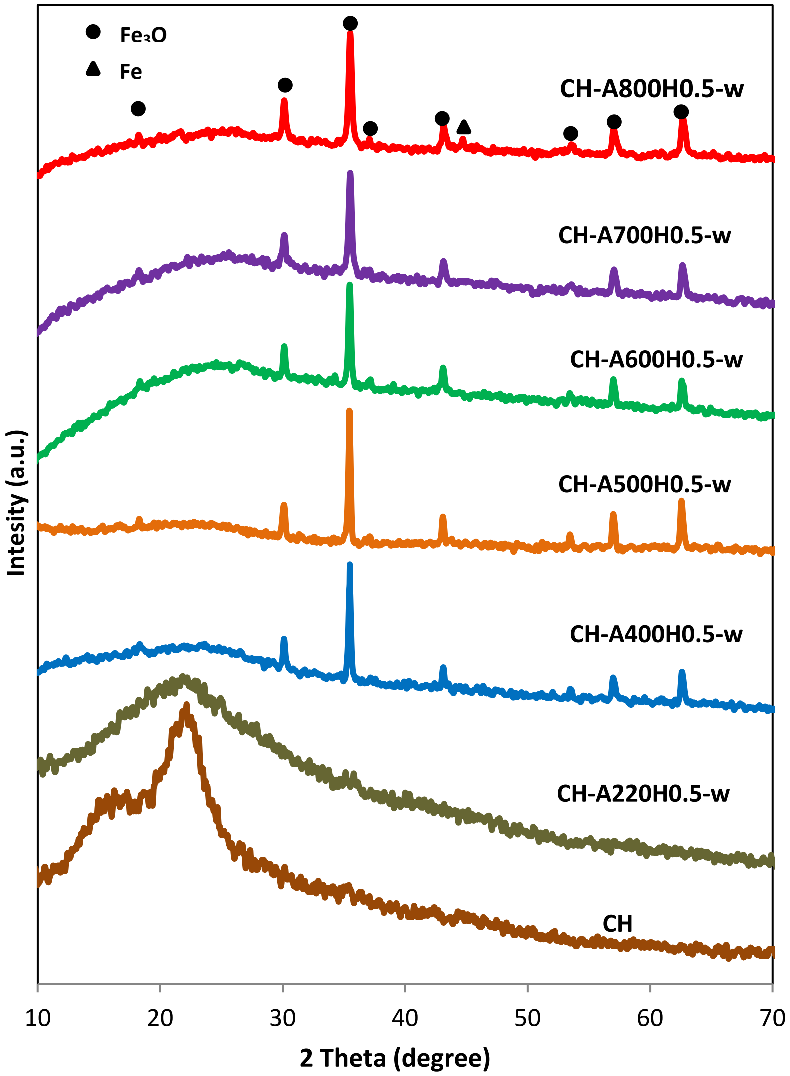

Fig.1 X-ray diffraction (XRD) of the CH and MACs obtained at different temperatures.

Bragg peak positions are indicated on the top of the figure for the different Fe_3O_4 and Fe crystal structures.

FTIR spectra of the evolution of structural features of CH and MACs are shown in Fig. 2. Additionally, to help in the location of the main absorption bands of magnetite, its spectrum is also displayed in Fig.2. The spectrum of CH is characterized by features common to lignocellulosic biomass and the assignments of main absorption bands corresponding to different functional groups are also depicted in Fig. 2 based on previous studies[36].

The FTIR results show that the raw CH suffer some chemical changes which are linked to the activation temperature. Obviously, the MAC activated at 220 ºC has the most recognizable absorption bands attributed to the raw CH, and the most significant changes at the lowest temperature are due to the loss of the less thermally stable functional groups, which leads to the release of relatively low molecular weight substances. In comparison with CH, it can be clearly observed that the absorbance characteristics assigned to the oxygen-containing groups are more affected. These chemical changes are linked to a decrease in the strong band due to the stretching vibration of hydrogen bonded O-H around 3400 cm^{-1} (νO-H), a slight decrease in carbonyl groups at 1740 cm^{-1} (νC=O) and C-O bonds in the range 1300–1000 cm^{-1} (νC-O) together with a decrease in the stretching and deformation vibrations of C-H bonds in aliphatic groups (3000-2800 cm^{-1} and 1475-1350 cm^{-1}, respectively). For the MACs series with the increase of activation temperature from 220 to 800 °C, the structural organic components, polysaccharides and lignin, occur in abrupt changes which are reflected in the variation of intensity, location and shape of the absorption bands. As temperature increases there is almost complete loss of C=O functionalities (1740 cm^{-1}) and the formation of new components in MACs. A gradually deoxygenation of the precursor and, consequently of the MACs, occurs as the activation temperature increases, becoming deeper at the highest temperature. This is in line with less H, less O, and more C in the elemental composition (Table 1). Likewise, some absorption bands below 900 cm^{-1} appear which are presented in the magnetite spectrum, Figure 2. Especially remarkable is the intense band at approximately 575 cm^{-1} assigned to Fe-O in iron oxide and in the magnetic substances, suggesting the presence of a certain iron oxide and magnetite[37-38]. The MACs obtained at 400, 500, 600, 700 and 800ºC presented two characteristic bands at 565 and 450 cm^{-1}, being the absorption band at 565 cm^{-1} the most significant at temperatures of 700 and 800ºC. These absorption bands are similar to those found in the Ying-Sing works[39-40] where they are attributable to the formation of hematite(α-Fe_2O_3) and the IR spectral analysis reveals that the magnetite is converted to, α-Fe_2O_3 at 500ºC and above[39]. In **Fig. 2,** at 700 and 800ºC a shoulder over 655 cm^{-1} is appreciated in the band at 565 cm^{-1}, and is similar to that found in magnetite-Fe_3O_4 in previous investigations, while the distinct high-frequency shoulder at 635 cm^{-1} is close to that of maghemite, γ-Fe2O3[41]. Further on, **Table 2** and **Fig. 4** reflect the results provided by the Mössbauer spectroscopy where for MACs obtained at 700 and 800ºC the presence of γ-Fe_2O_3 is confirmed.

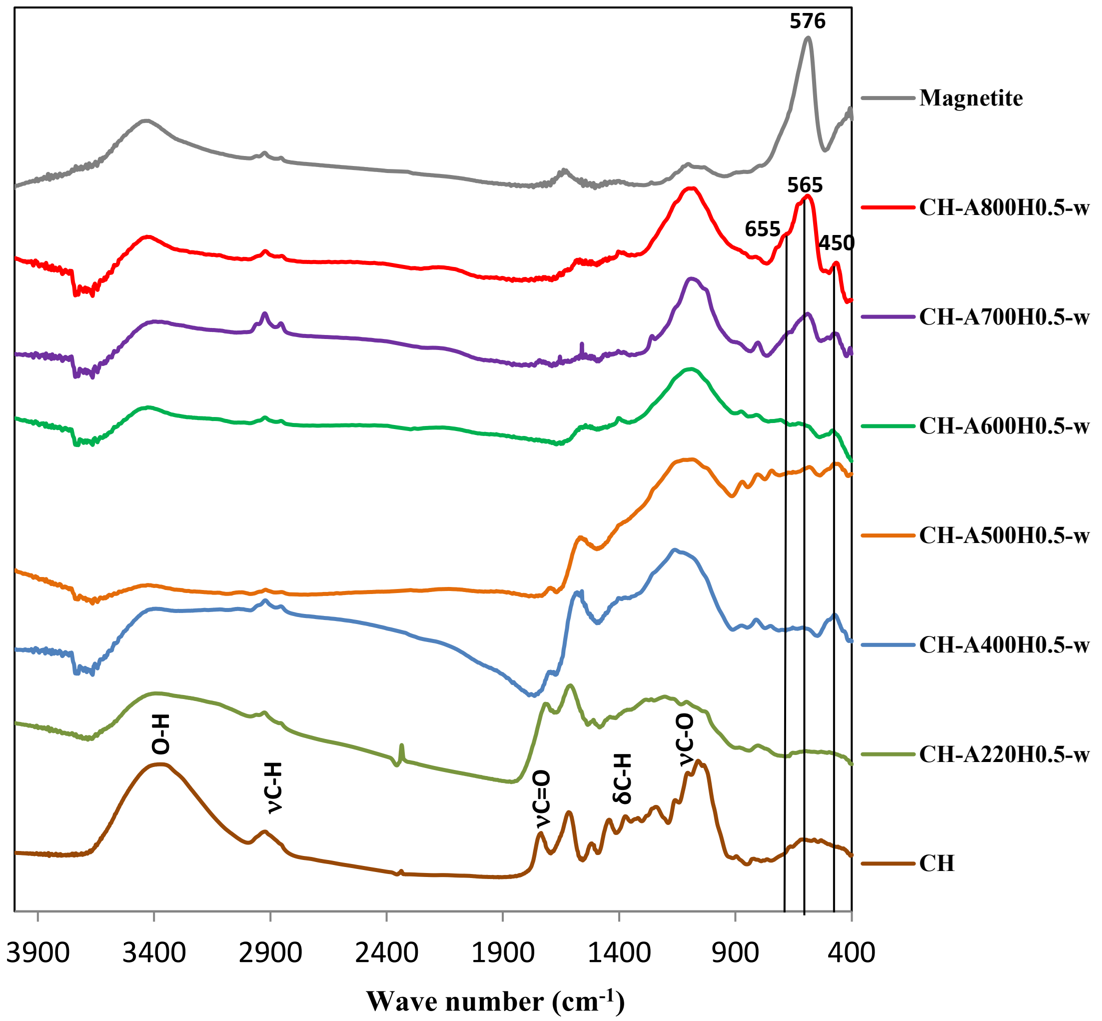

Fig. 2. FTIR spectra of the CH, the MACs obtained at different temperatures and the magnetite.

The structure features of the carbon layer in the CH and CH-based MACs were detected by Raman spectroscopy. In **Fig. 3** two Raman characteristic peaks in the carbonaceous materials are observed in the MACs obtained: Peak at 1350 cm^{-1} wich is induced by structural defects associated with graphitic disorder[42] (D-band) and the second one at 1580 cm^{-1} which corresponds to in-plane vibrations of sp2-bonded carbon atoms observed for graphite crystals[43] (G-band). The peak appearing at 1300 cm^{-1} in the magnetite spectrum, **Fig. 3**, contributed to the widening to the D-band presented in the

CH baed-MACs. None of these peaks are observed in the case of the raw material. In the MAC obtained at 220ºC the D-band was not completely developed and seems to be a shoulder of the G-band. They are very closely and the D-band is lower and less defined. This effect also happens in Rufford et al. research[44], where the intensity of the D peak of the samples treated at 300ºC is lower than that of the MACs obtained at 900ºC . Also, in the Gong et al. work[14], Raman bands peaks for MACs obtained at 400ºC were not well-defined, due to the incomplete carbonization as a consequence of the low activation temperature. Furthermore, the structural disorder reflected in the Raman D-band at higher temperatures could indicate the increase of the microporosity in the material[44].

The Raman spectra of MACs obtained from 400ºC to 800ºC showed small peaks that were detected at 223, 287, 402 and 599 and 637 cm^{-1} and they are very similar to those presented in the magnetite spectrum, **Fig.3**. This magnetite spectrum resembles that which appears in the Alvear et al. work[45].

The raw material and the sample CH-A220H0.5-w did not present these peaks and their spectra were very similar in this range. Besides these bands showed more intensity depending on which areas of the material are illuminated: magnetite crystals or carbonaceous material. These peaks indicated the presence of magnetite and iron oxides [38, 46]. In MACs obtained at 700 and 800ºC seems to decrease the intensity of the characteristic peaks of the magnetite, due to the evolution of the magnetic species presented in those materials towards other iron species as it was indicated by the Mössbauer analysis in the **Table 2** and **Fig.4**.

It is worth nothing that Raman is used in this work to support other more common techniques employed in the study of MACs.

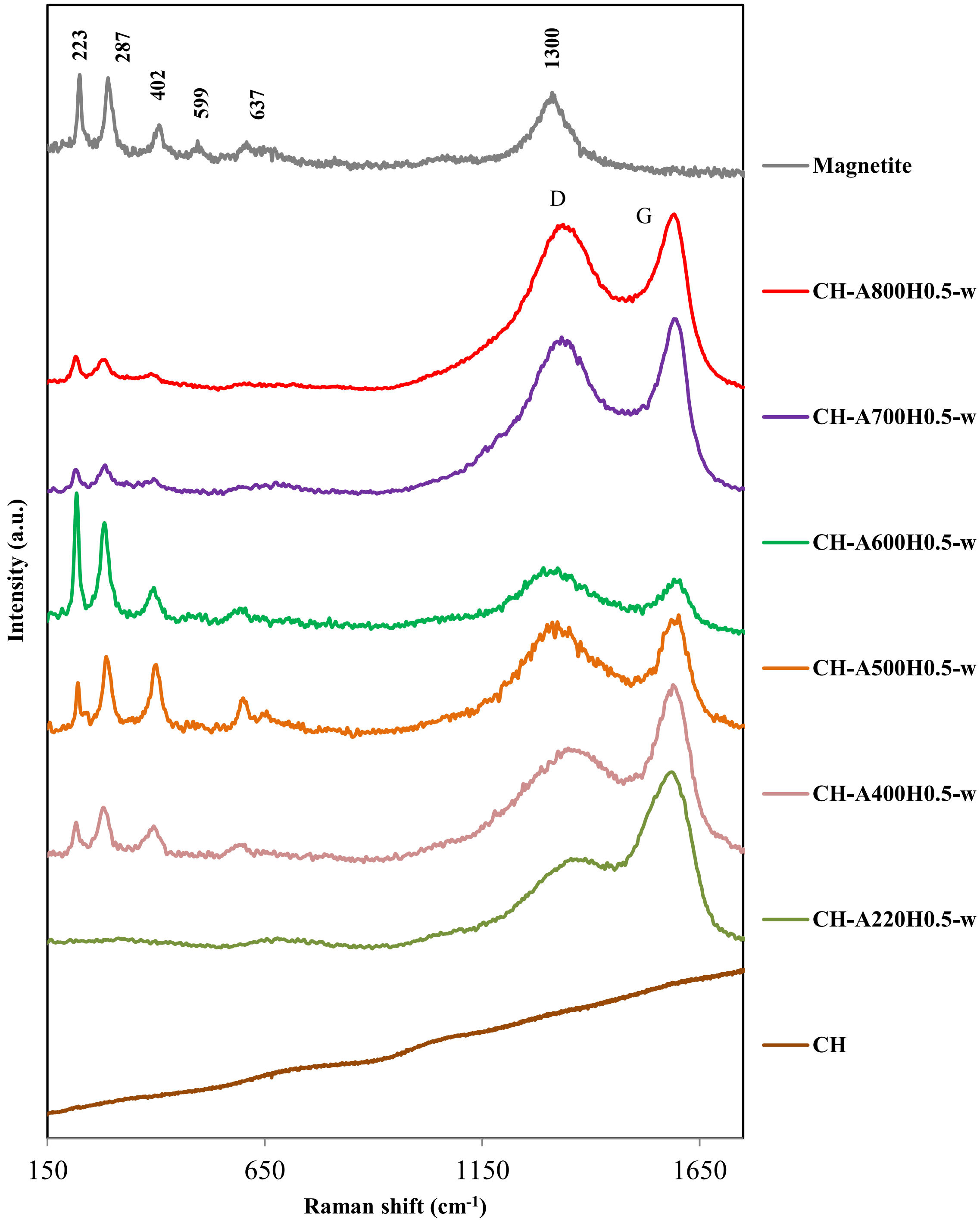

Figure 3. Raman spectra of the CH, the MACs obtained at different temperatures and the magnetite..

A deeper analysis of the iron species is performed by Mössbauer spectroscopy. **Figure 4** shows the Mössbauer spectra recorded for all the samples considered in this paper. The spectrum corresponding to sample CH-A220H0.5-w is characterized by a very low absorption resulting from its very small iron concentration (**Table 1**). The spectrum consists in a single paramagnetic doublet with Mössbauer parameters (δ=0.37 mms^{-1}; Δ=0.85 mms^{-1}) which are typical of Fe^{3+} in distorted oxygen octahedral coordination and probably arises from the presence of small particle Fe^{3+}-containing oxides[47]. The spectrum has very broad lines what is compatible with the occurrence of a multiplicity (distribution) of Fe^{3+} ions in slightly different distorted octahedral environments. The result is compatible with the presence of chemical inhomogeneities/disorder in the sample and correlates well with its XRD data (**Fig. 1**) which only show a broad background with no evident diffraction reflections.

The spectra recorded for samples CH-A400H0.5-w, CH-A500H0.5-w and CH-A600H0.5-w contain two sextets and a paramagnetic Fe^{3+} doublet. The Mössbauer parameters of the two sextets (δ_A=0.30 mms^{-1}; 2ε_A=0.02 mms^{-1}; H_A=48.6 T; δ_B=0.66 mms^{-1}; 2ε_B=-0.01 mms^{-1}; H_B=45.2 T) are characteristic of the Fe^{3+} tetrahedral (A) and $Fe^{2.5+}$ octahedral (B) sites of magnetite (Fe_3O_4)[47] while the parameters of the doublet are very close to those observed for the doublet of the first sample and, therefore, it can be associated with the presence of superparamagnetic Fe^{3+}-containing oxides. The B/A sextet area ratio is around 1.0 what indicates that magnetite is non-stoichiometric. The relative contributions of these two iron species vary from sample to sample, their respective percentages being collected in **Table 2**.

The spectrum corresponding to sample CH-A700H0.5-w is rather more complex. The spectrum also contains magnetite and paramagnetic components but in addition to those it has a maghemite (γ-Fe_2O_3) contribution (δ=0.31 mms^{-1}; $2\varepsilon_A$=0.02 mms^{-1}; H_A=49.8 T) and two other broad, minor magnetic contributions which have a more difficult assignment on the basis of their Mössbauer parameters (δ=0.41 mms^{-1}; $2\varepsilon_A$=0.08 mms^{-1}; H_A=42.1 T and δ=0.37 mms^{-1}; $2\varepsilon_A$=-0.10 mms^{-1}; H_A=32.7 T). Since their isomer shifts are characteristic of Fe^{3+} and they have relatively low hyperfine magnetic field values they could be associated with nanophasic iron oxides. **Table 2** collects the relative contributions of each iron phase to this sample.

Finally, the spectrum recorded from CH-A800H0.5-w is, by far, the most complex of all the samples. It contains non-stoichiometric magnetite, maghemite, a small paramagnetic Fe^{3+} contribution, a component assignable to a nanophasic iron oxide, metallic iron (δ=0.00 mms^{-1}; $2\varepsilon_A$=0.00 mms^{-1}; H_A=33.0 T) and the iron carbide, Fe_3C, cementite (δ=0.17 mms^{-1}; $2\varepsilon_A$=0.00 mms^{-1}; H_A=20.8 T)[48]. The relative concentrations of each species are collected in **Table 2**.

Table 2-Relative contributions of the different iron phases identified by Mössbauer spectroscopy

Sample	Relative spectral area (%)						
	Paramagnetic Fe^{3+}	Fe_3O_4	γ-Fe_2O_3	Nanophasic Fe^{3+} oxide	Nanophasic Fe^{3+} oxide	Metallic iron	Fe_3C
CH-A220H0,5-w	100	---	---	---	---	---	---
CH-A400H0,5-w	45	55	---	---	---	---	---
CH-A500H0,5-w	23	77	---	---	---	---	---
CH-A600H0,5-w	33	67		---	---	---	---
CH-A700H0,5-w	23	39	18	8	12	---	---
CH-A800H0,5-w	4	39	10	7	---	30	10

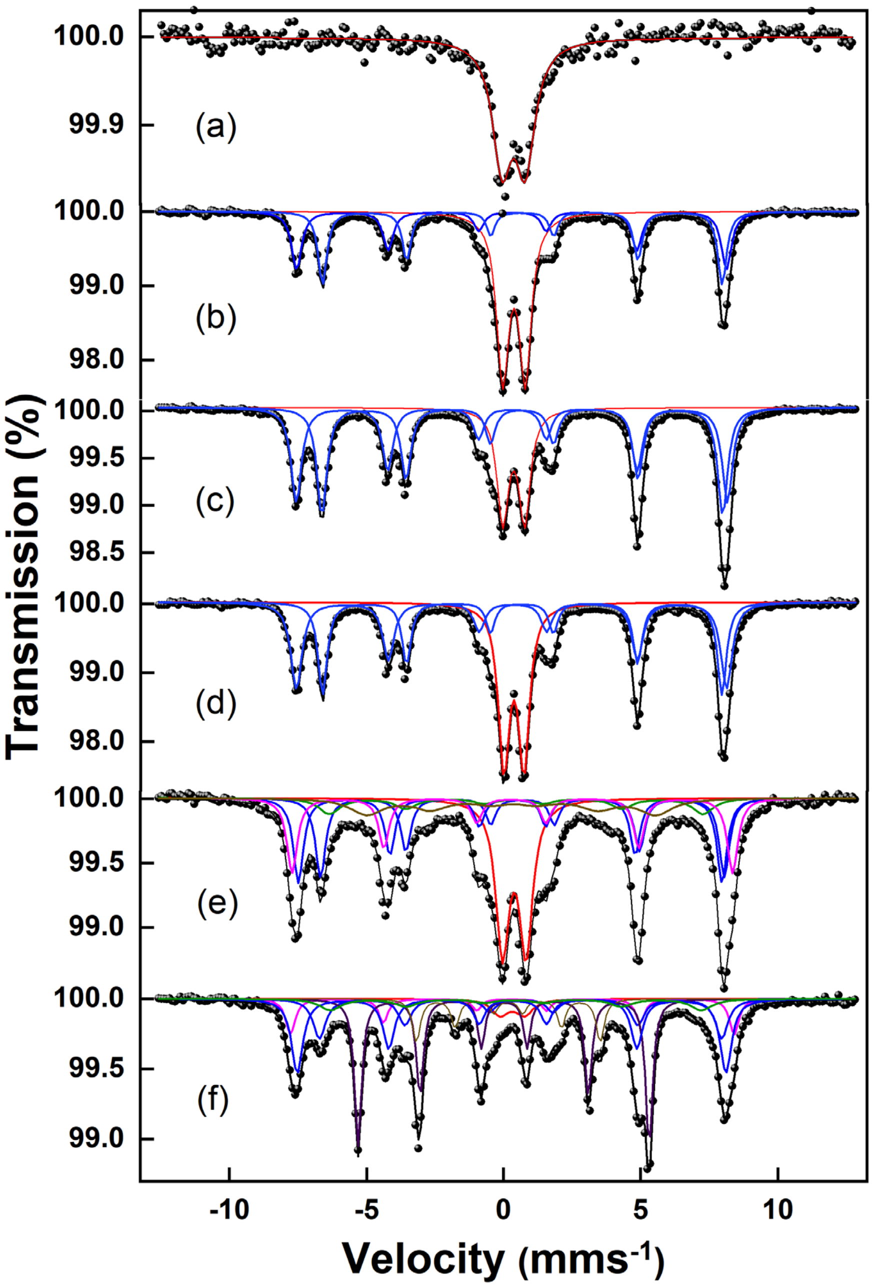

Figure 4. Room temperature Mössbauer spectra recorded from (a) CH-A220H0.5-w, (b) CH-A400H0.5-w, (c) CH-A500H0.5-w, (d) CH-A600H0.5-w, (e) CH-A700H0.5-w and (f) CH-A800H0.5-w.

Morphology and Structure of the materials. Some SEM photographs taken at different magnifications of the raw material (CH) and the chestnut shell wastes-based magnetic activated carbons are shown in Fig 5. Pictures corresponding to MACs present significant differences or similarities in their morphology between them and with the raw material depending on the temperature.

SEM observations of the CH raw biomass reveals the presence of irregularly-shaped, compact and hard particles with fibrous material (Fig. 5 a). When a soft activation at 220 °C is applied, the MAC obtained did not present any appreciable singularity except the appearance of some holes or cavities in the surface. This effect is better appreciated in the Oliveira et al. study[8] where the MACs obtained from coffee husks by impregnation with ferric chloride presented surface craters with thinner walls in the materials activated at 280ºC and probably favored by the presence of iron species in their preparation.

In the present work, MACs prepared at temperatures greater or equal than 400ºC showed cavities and channels more developed and more numerous than in MAC obtained at 220ºC indicating the generation of porosity although some of these pores could be occupied or blocked by the iron compounds formed.

In the EDX analysis of the sample CH-A220H0.5-w, **Fig. 5 b)** the iron atomic percentage indicated was insignificant (<0.1%) and no iron compounds were observed. On the other hand, the carbon atomic percentage in this material remained high (72.46%) as the studied area showed. These results are in line with those obtained in the elemental analysis of this material (**Table 1**) which presented a carbon content of 58.90% and Fe of 1.06%.

At temperatures greater or equal than 400ºC, cavities and channels more developed and more numerous were visible in the obtained MACs indicating the generation of porosity although some of these pores could be occupied or blocked by the iron compounds formed.

In the MAC obtained at 400ºC, CH-A400H0.5-w, **Fig. 5 c)**, showed some iron oxide crystals deposited on the surface of the samples with a well-defined shape and they could be attributed to magnetite crystals as confirmed Mössbauer, Raman, XRD analysis. Iron atomic percentage increased and the carbon percentage decreased respect to the material carried out at 220ºC and these results were reflected in the EDX analysis of the crystals formation which were analyzed, **Fig. 5c)**.

The images corresponding to the sample CH-A800H0.5-w, **Fig. 5d)** showed that these crystals formed at lower temperatures (400-600ºC) had changed and a conglomerate of iron compounds was formed similar to the aggregated iron oxide particles observed on the surface of MACs reported by different authors[10, 14, 23]. As can be seen in the areas analyzed, **Fig. 5d)**, a high percentage of atomic iron is detected, up to 28.82% (up to 62.56 wt% Fe), being upper than the atomic iron percentage values presented by MACs obtained at a lower activation temperature.

This high iron percentage in CH-A800H0.5-w is also reflected in chemical composition, so that this material presented a higher iron content (23.46%) than the MACS obtained at a lower temperature (up to 16.69%). Mössbauer analysis also indicated that this material had the highest number of iron compounds, including iron carbide and metallic iron that do not appear in any of the other materials.

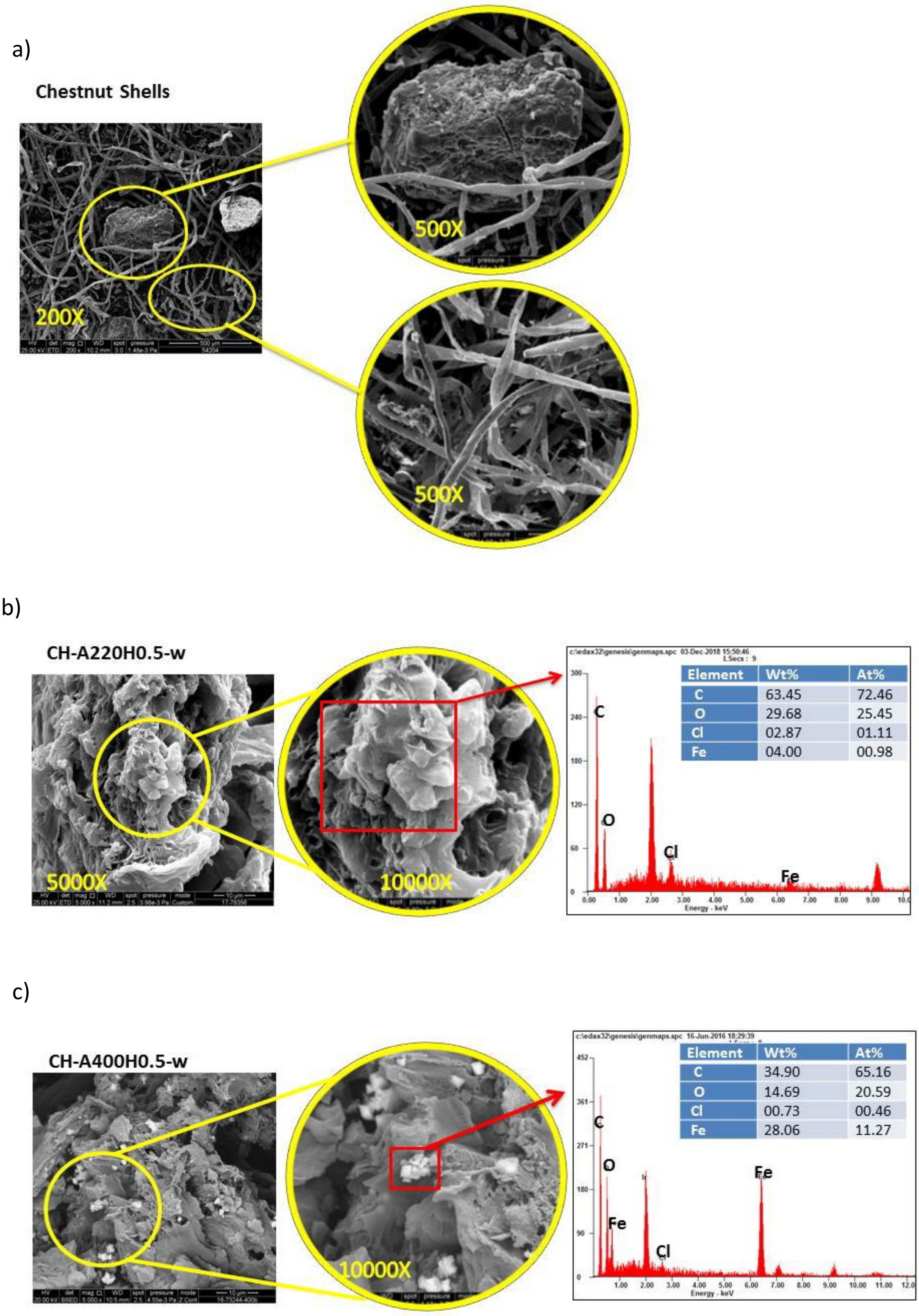

a)
Chestnut Shells
200X
500X
500X
b)
CH-A220H0.5-w
5000X
10000X
Element Wt% At%
C 63.45 72.46
O 29.68 25.45
Cl 02.87 01.11
Fe 04.00 00.98
C
O
Cl
Fe
Energy - keV
c)
CH-A400H0.5-w
10000X
Element Wt% At%
C 34.90 65.16
O 14.69 20.59
Cl 00.73 00.46
Fe 28.06 11.27
C
O
Fe
Cl
Fe
Energy - keV

d)

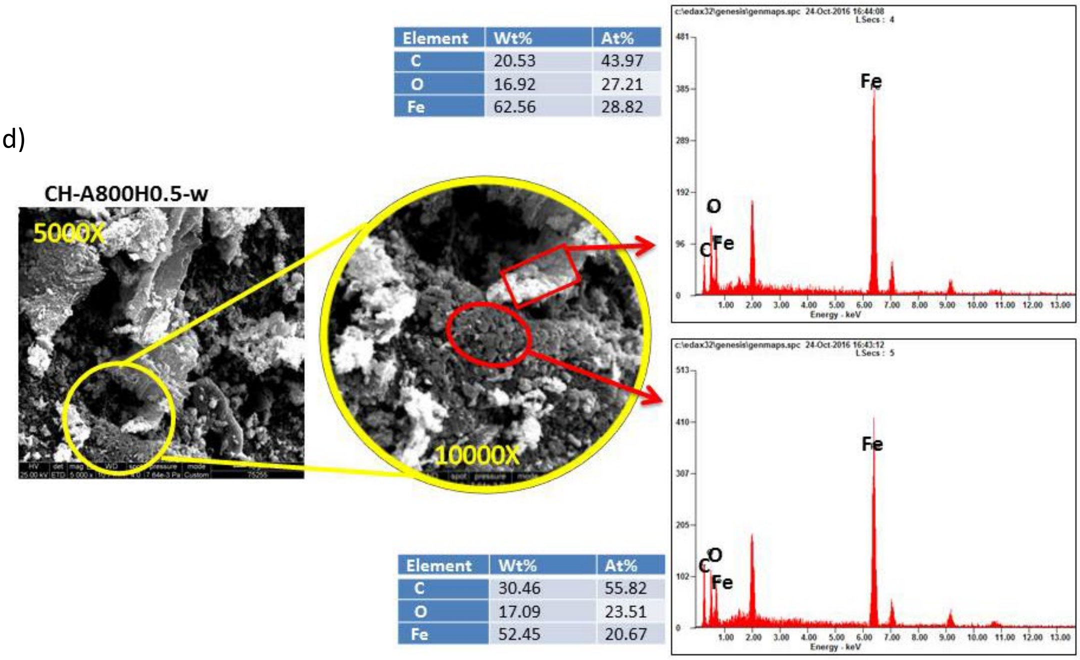

Figure 5. SEM photographs of a) CH; b) CH-A220H0.5-w; c) CH-A400H0.5-w; d) CH-A800H0.5-w

Textural properties. The textural parameters data (S_{BET}, V_{TOT} and the pore size distribution –PSD-) are shown in **Table 3**. The real density of the materials is the helium density and in the present work increases from 1.43 g cm^{-3} for the chestnut shells waste to 2.40 g cm^{-3} for the MAC at 800ºC. The value is slightly higher than in activated carbons from the same lignocellulosic industrial biomass waste described in B. Ruiz et al work[24]. The higher the activation temperature, the higher the order of the material, and therefore, the higher the helium density.

N_2 adsorption isotherms at -196°C are presented in **Fig.6**. MACs obtained at temperatures equal o higher at 400ºC present a significant amount of adsorbed N_2 at low pressures, which increases as the activation temperature increases. The isotherms of these materials present a hybrid form between types I-IV according to the IUPAC classification, with a cycle of incipient hysteresis, which is perfectly developed in the material activated at 800ºC (type H4), indicating the presence of mesoporous in this material. For activated carbons developed in our research group using the same biowaste but with KOH activation and preceded by a pyrolysis step, the isotherms are type I and have a higher nitrogen adsorption (more than double) [24].

The magnetite hardly presents adsorption of N2 at -196ºC and in the isotherm a cycle of hysteresis type H3 can be appreciated as it is described in Thommes et al. work[49].

The raw material and the MAC obtained at 220°C are very similar with a negligible nitrogen adsorption and low BET surface area (≤ 3 m^2/g) and porosity, **Fig.6** , **Fig.DFT**, **Table 3**. The SEM images of these materials confirm the absence of significant porosity in these samples (**Fig.5a), 5b)**)

In this work the material obtained at 220°C did not present textural development in contrast with Oliveira et al. [8] research, where samples obtained using ferric chloride as activating agent at 280ºC in ACs preparation from coffee husks were suitable as adsorbents for cationic dyes and phenol.

The highest BET surface area reached at 800ºC was 568 m^2/g, **Table 3**, better than those found in other research works[29-30] but lower than the values (1100-1790 m^2/g) of the activated carbons developed in our research group using the same biowaste although with KOH activation and preceded by a pyrolysis step[24]. This result may be due, on the one hand, to the formation of iron compounds nanoparticles in surface and inside the porous structure of the MAC obtained blocking porosity which could cause a reduction in the amount of nitrogen adsorption, BET surface area and porosity as reflected in the work of Do et al. [35]. Another one of the causes is that these MACs obtained presented high ashes content (up to 34.50%) that do not contribute to the total porosity of the magnetic adsorbent materials. The total pore volume obtained at p/p^0 of 0.99 follows a trend similar to the BET surface area increasing from 0.017cm^3/g for the MAC obtained at 220°C to 0.294 cm^3/g for the MAC at the highest temperature, **Table 3**.

The PSD showed the existence of microporosity in the MACs obtained from 400ºC (micropore volume up to 0.133 cm^3/g for CH-A800) and in general with a greater presence of ultramicropores (pore width <0.7 nm) up to 0.081 cm^3/g for MAC obtained at 600ºC; on the other hand, there is a small contribution of mesopores that generally increases with the activation temperature until reaching the value of 0.033 cm3/g in the MAC obtained at 800°C (**Fig DFT** and **Table 3**).

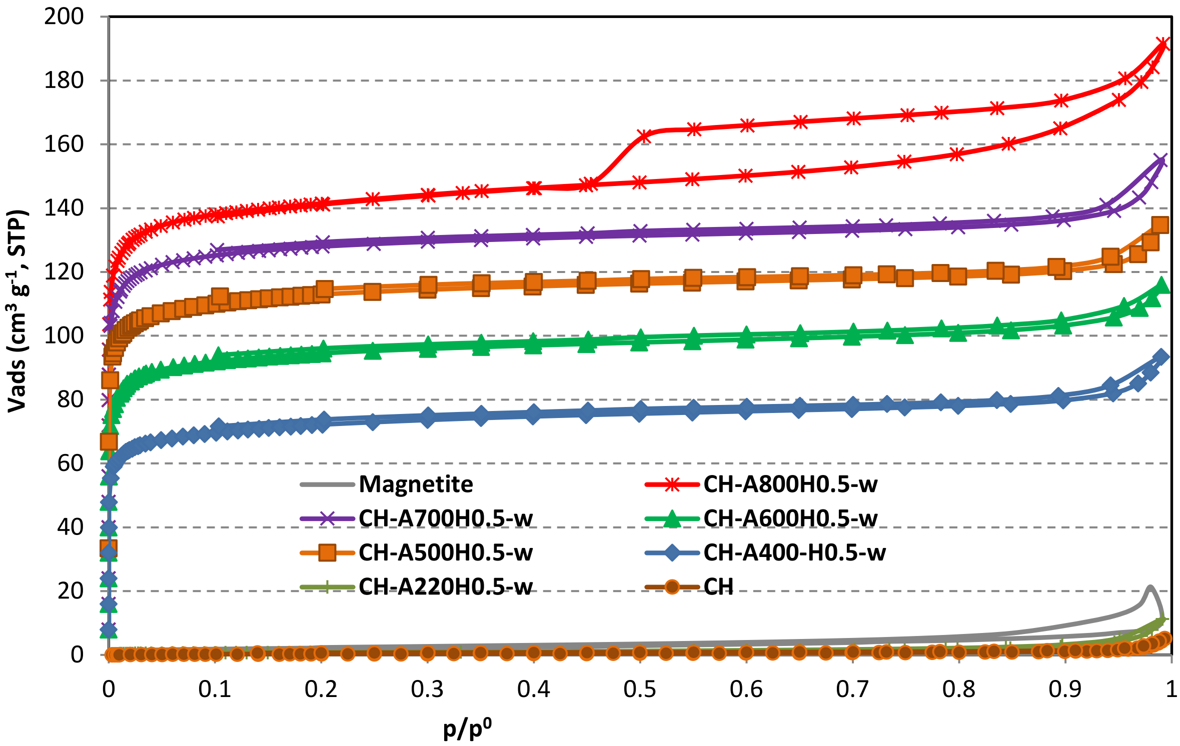

Figure 6. N_2 isotherms at -196ºC for the raw material (CH), the MACs and the magnetite

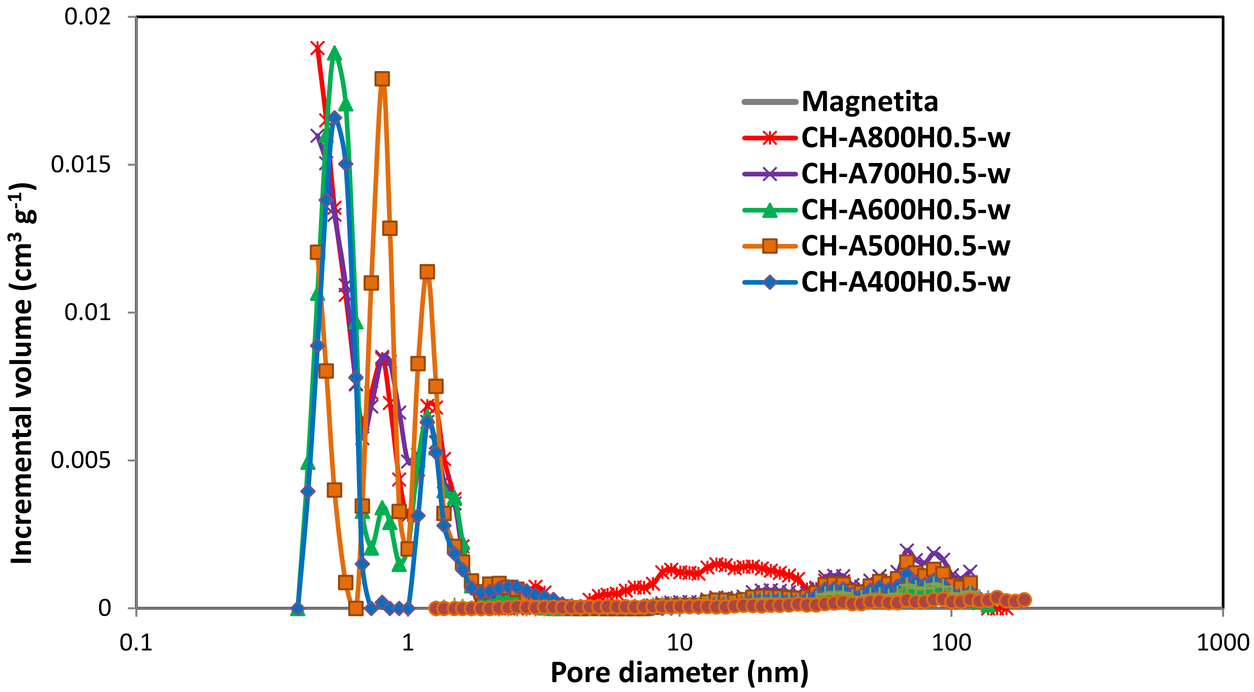

Figure DFT. Incremental pore volume versus pore width based on the N_2 isotherms of the biomass waste, MACs and the magnetite.

Table 3. Textural parameters of the materials.

Sample Ref.	ρHe g·cm^{-3}	N_2 asorption at -196°C					CO_2 adsorption at 0°C				
		S_{BET} m^2·g^{-1}	V_{TOT} cm^3·g^{-1} p/p^0=0.99	*Vumi cm^3·g^{-1} <0.7nm	*Vmmi cm^3·g^{-1} 0.7-2nm	*Vme cm^3·g^{-1} 2-50nm	W_0 cm^3·g^{-1}	S_{DR} m^2·g^{-1}	E_0 KJ·mol^{-1}	L_0 nm	S_{mi} m^2·g^{-1}
CH	1.43	1	0.007	0.000	0.000	0.003	0.048	125	23.36	0.90	106
CH-A220H0.5-w	1.48	3	0.017	0.000	0.000	0.007	0.078	203	26.50	0.72	217
CH-A400H0.5-w	1.69	285	0.145	0.068	0.023	0.011	0.183	479	28.91	0.62	594
CH-A500H0.5-w	1.71	451	0.209	0.033	0.079	0.012	0.213	558	28.20	0.64	663
CH-A600H0.5-w	1.90	380	0.179	0.081	0.039	0.008	0.219	572	28.49	0.63	692
CH-A700H0.5-w	2.10	518	0.241	0.071	0.061	0.014	0.238	623	27.17	0.68	694
CH-A800H0.5-w	2.40	568	0.294	0.076	0.057	0.033	0.198	519	27.22	0.68	580
Magnetite	4.63	8	0.034	0.000	0.000	0.009	0.002	6	27.92	0.65	7

*Vumi: Vultramicropores (volume corresponding to pore width <0.7 nm).
*Vmmi: Volume medium-micropores (volume corresponding to pore width 0.7-2nm).
*Vme: Volume mesopores (volume corresponding to pore width 2-50 nm.)

CO_2 adsorption isotherms at 0°C are used in ACs works[5, 24] to study the narrow microporosity (pore width smaller than 0.7 nm) and to calculate the micropore volume

(W_0), energy characteristic (E_0) and micropore size (L_0) applying the Dubinnin-Raduskevich equation. However, it is an unusual technique in the characterization of MACs as N_2 adsorption is commonly employed to study textural properties. This analysis was carried out to study the activation temperature influence in the ultramicroporosity development of MACs and complement studies of textural characterisation by N_2 adsorption. In **Fig.7**, the CO_2 isotherms at 0°C of the materials obtained in this work are presented and **Table 3** shows the values of the textural parameters obtained from these isotherms. The raw material and the MAC obtained at the lowest activation temperature (220ºC) have a very similar behaviour although the activated one presented a little more adsorption (**Fig.7**). Likewise, the values for the sample activated at 220ºC increased slightly with respect to the original biomass: W_0 up to 0.078 cm^3/g, S_{DR} up to 203 m^2/g and S_{mi} up to 217 m^2/g. The micropore size of the biomass waste was 0.90 nm. During the activatation process was generated ultramicropore volume and the MAC obtained at 200°C presented a pore size of 0.72 nm (**Table 3**). In general, with activation temperature ≥400°C, MACs obtained presented a higher CO2 adsorption, **Fig.7**.

the micropore volume (W_0) increases with temperature up to maximum value of 0.238 cm^3/g for the MAC obtained at 700°C, but when the activation temperature is 800°C this value decreases to 0.198 cm^3/g which may be due to the collapse of adjacent pore walls. In fact, this may explain why the pore size is wider at higher activation temperatures (0.062 nm for CH-A400 v.s. 0.68 nm for CH-A700 and CH-A800) and very similar to the results obtained at the same temperature range in Ruiz et al study[24] where the same biowaste was pyrolyzed and activated with KOH. The S_{DR} (up to 623 m^2/g) and S_{mi} (up to 694 m^2/g) at 700ºC are also the highest values obtained in the present work, as it happens at 750ºC in Ruiz et al study[24].

Finally, as can be seen in the **Table 3** and **Fig.7**, the magnetite presented a negligible adsorption of CO_2.

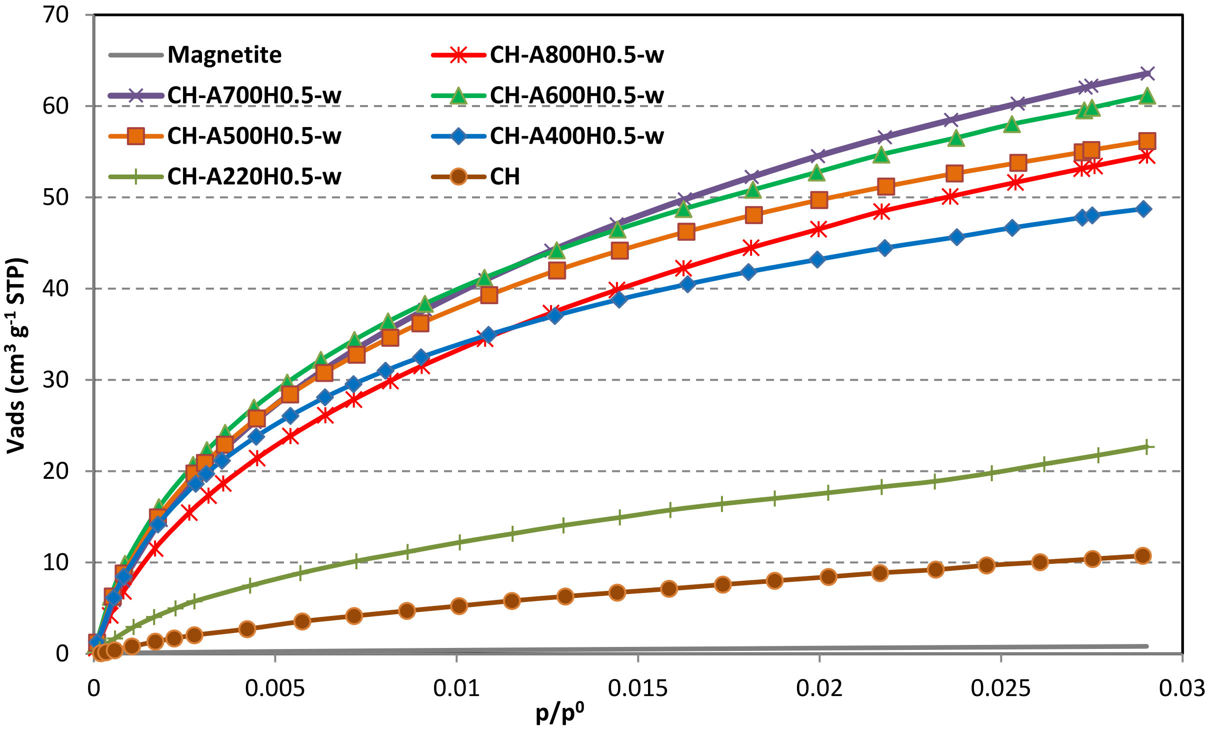

Figure 7. CO_2 isotherms for the raw material (CH), the MACs and the magnetite.

Magnetic properties **Figure 8** shows the field dependence of the magnetization M(H) at RT where hysteretic magnetic properties such as remanent magnetization, M_R, and coercivity, H_c, are depicted in the inset. It is worth noting that the lowest activation temperature (220ºC) only modifies the diamagnetic nature of the raw material (CH) to a paramagnetic substance, characterized both by a linear response of M(H) but with negative or positive slope, respectively. Above this temperature, the rest of samples seem to be ferromagnetic, the largerM_R and H_c , the higher activation temperature, **Table 4**. In addition, the value of saturation magnetization, M_S, can be estimated from the high magnetic field region of the M(H) curves using the following approach-to-saturation law[50]:

$$M = M_S \cdot \left(1 - \frac{a}{H} - \frac{b}{H^2}\right) + \chi \cdot H \tag{1}$$

showed similar trend that previous magnetic parameters. Besides that, taking into account the iron content of every sample (**Table 1**) and different relative contributions of each phases identified by Mössbauer spectroscopy (**Table 2**), we can explain the saturation magnetization values. Thus, the increase in the ratio between magnetite and paramagnetic phases along the increase in the iron amount are both mainly responsible for the rising in M_S observed for the samples CH-A400H0.5-w, CH-A500H0.5-w and CH-A600H0.5-w. Furthermore, the formation of metallic iron at the highest activation temperatures leads to an extra increase of M_S due to its higher saturation magnetization value (217 emu/g) compared to that of magnetite (92 emu/g)[51]. Moreover, coexistence of different ferromagnetic phases and size-dependence effects could be the cause of the increase in coercivity reported.

Table 4. Magnetic parameters (M_R, remanent magnetization; H_C, coercivity; saturation magnetization, M_S; a and b parameters in eq. (1), magnetic susceptibility, χ) obtained from the hysteresis loops.

Sample	**M_R [emu/g]**	**H_C [emu/g]**	**M_S [emu/g]**	***a*** **[10^2 Oe]**	***b*** **[10^6 Oe^2]**	**χ [10^{-6} emu/g·Oe]**
CH	-	-	-	-	-	-0.28·
CH-A220H0.5-w	-	-	-	-	-	1.61
CH-A400H0.5-w	0.15	45	2.9	-0.862	1.19·	5.50
CH-A500H0.5-w	0.40	33	9.0	-0.365	8.23·	4.60
CH-A600H0.5-w	0.72	65	10.0	-1.92	1.56·	11.04
CH-A700H0.5-w	1.59	97	17.8	-1.23·	1.63·	6.19
CH-A800H0.5-w	3.88	140	30.78	-1.92	1.56·	11.04

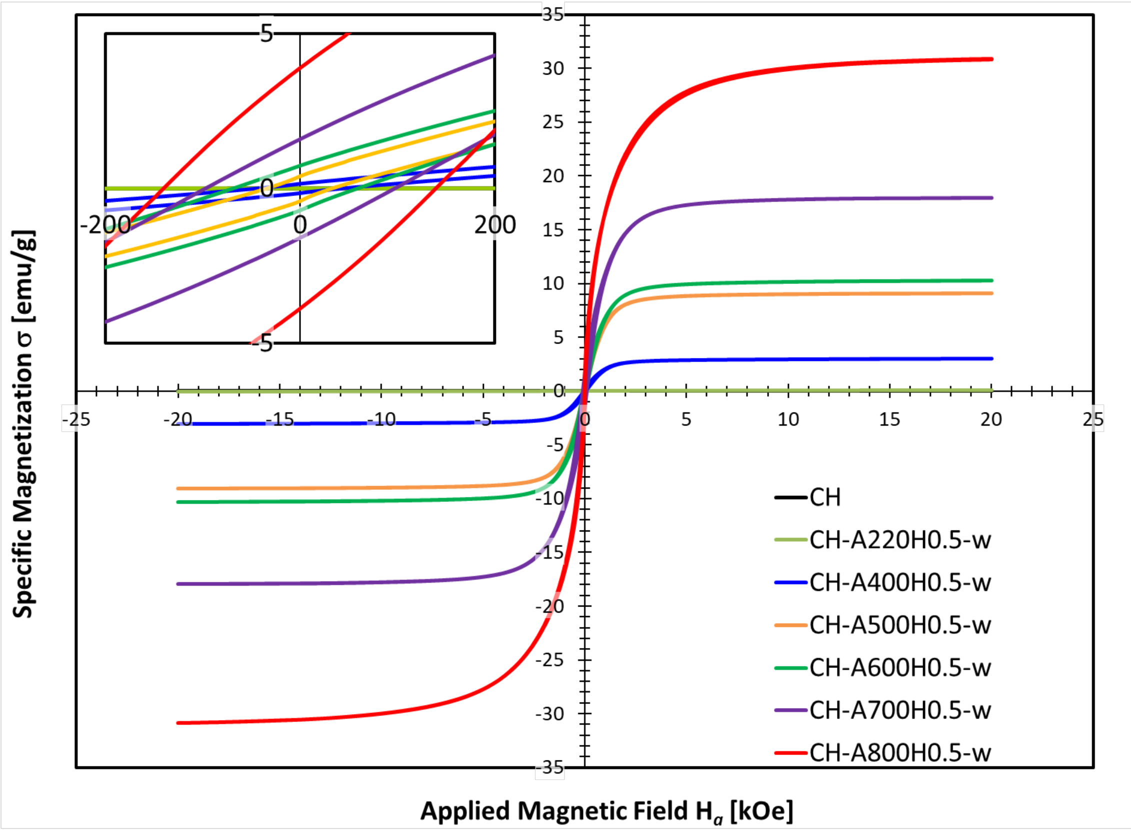

Figure 8. Field-dependence of magnetization M(H) at room temperature**.** The inset depicts the central area of the loops.

▪ CONCLUSIONS

- Optimization of the process for obtaining MACs. A new technique for obtaining this type of material through a single-stage thermochemical process, bringing the waste (chestnut shell) into contact with the activating agent by a direct mixing, has been confirmed with good results.

- The activation temperature has an important influence on the chemical composition of the MACs. As the temperature increases, so does the percentage of carbon and iron, but the percentage corresponding to oxygen and hydrogen decreases.

- The analysis techniques used : DRX, FTIR, RAMAN and Mössbauer confirmed the presence of magnetite and the appearance of magnetic species, such as Fe oxides, carbides and even metallic Fe depending on the temperature at which the thermochemical process is carried out. The results showed the absence of these magnetic species at low activation temperature (220ºC).

- Effect of activation temperature on the morphology of materials, with the appearance of magnetic crystalline species from 400ºC and their evolution towards conglomerates at 800ºC.

- Influence of the activation temperature on the textural development and pore size of the materials obtained. The increase in activation temperature favours greater BET areas (up to 568 m^2/g) (with the exception of the sample obtained at 600ºC and the presence of microporosity (up to 0.133 cm^3/g) and some mesoporosity (up to 0.033 cm^3/g).

- MACs obtained at low temperature (220ºC) do not have the same characteristics as those obtained at higher temperatures. The magnetic species are absent, as indicated by all the instrumental techniques used and the textural development is insignificant (S_{BET}: 3 m^2/g).

-Mössbauer

- Magnetic properties of the MACs are improved as the activation temperature increase because of nucleation, growth, structure transformation and interactions between the different iron base phases determine on the analysis techniques used.

▪ SYNOPSIS

Industrial biowastes MACs obtained through an optimized single-step thermochemical process in a results in a more sustainable and economical process with interesting data depending on the activation temperature used.

▪ ACKNOWLEDGEMENTS

The financial support for this work was provided by the Plan Nacional, Ministerio de Economía y Competitividad of Spain: PN (MINECO), under the Project CTM2014-58435-C2-1-R. The authors also acknowledges to Alejandra Carranza for her collaboration in in the process of MACs obtention.. The scientific and Technical Services (SCTs) at the University of Oviedo are acknowledged as well as the project RTI2018-094683-B-C52.

▪ REFERENCES

1. Reinoso, H. M. F. R., Activated Carbon. **2006,** *1st Edition*.
2. González-García, P., Activated carbon from lignocellulosics precursors: A review of the synthesis methods, characterization techniques and applications. *Renewable and Sustainable Energy Reviews* **2018,** *82*, 1393-1414.
3. Gil, R. R.; Ruiz, B.; Lozano, M. S.; Martín, M. J.; Fuente, E., VOCs removal by adsorption onto activated carbons from biocollagenic wastes of vegetable tanning. *Chemical Engineering Journal* **2014,** *245* (Supplement C), 80-88.
4. Lladó, J.; Gil, R. R.; Lao-Luque, C.; Solé-Sardans, M.; Fuente, E.; Ruiz, B., Highly microporous activated carbons derived from biocollagenic wastes of the leather industry as adsorbents of aromatic organic pollutants in water. *Journal of Environmental Chemical Engineering* **2017,** *5* (3), 2090-2100.

5. Lopez-Anton, M. A.; Gil, R. R.; Fuente, E.; Díaz-Somoano, M.; Martínez-Tarazona, M. R.; Ruiz, B., Activated carbons from biocollagenic wastes of the leather industry for mercury capture in oxy-combustion. *Fuel* **2015,** *142* (Supplement C), 227-234.
6. Ferrera-Lorenzo, N.; Fuente, E.; Suárez-Ruiz, I.; Ruiz, B., Sustainable activated carbons of macroalgae waste from the Agar–Agar industry. Prospects as adsorbent for gas storage at high pressures. *Chemical Engineering Journal* **2014,** *250* (Supplement C), 128-136.
7. Wong, S.; Ngadi, N.; Inuwa, I. M.; Hassan, O., Recent advances in applications of activated carbon from biowaste for wastewater treatment: A short review. *Journal of Cleaner Production* **2018,** *175*, 361-375.
8. Oliveira, L. C. A.; Pereira, E.; Guimaraes, I. R.; Vallone, A.; Pereira, M.; Mesquita, J. P.; Sapag, K., Preparation of activated carbons from coffee husks utilizing FeCl3 and ZnCl2 as activating agents. *Journal of Hazardous Materials* **2009,** *165* (1), 87-94.
9. Dai, J.; Tian, S.; Jiang, Y.; Chang, Z.; Xie, A.; Zhang, R.; Li, C.; Yan, Y., Fe3C/Fe/C Magnetic Hierarchical Porous Carbon with Micromesopores for Highly Efficient Chloramphenicol Adsorption: Magnetization, Graphitization, and Adsorption Properties Investigation. *Industrial & Engineering Chemistry Research* **2018,** *57* (10), 3510-3522.
10. Cazetta, A. L.; Pezoti, O.; Bedin, K. C.; Silva, T. L.; Paesano Junior, A.; Asefa, T.; Almeida, V. C., Magnetic Activated Carbon Derived from Biomass Waste by Concurrent Synthesis: Efficient Adsorbent for Toxic Dyes. *ACS Sustainable Chemistry & Engineering* **2016,** *4* (3), 1058-1068.
11. Hao, W.; Björnerbäck, F.; Trushkina, Y.; Oregui Bengoechea, M.; Salazar-Alvarez, G.; Barth, T.; Hedin, N., High-Performance Magnetic Activated Carbon from Solid Waste from Lignin Conversion Processes. 1. Their Use As Adsorbents for CO2. *ACS Sustainable Chemistry & Engineering* **2017,** *5* (4), 3087-3095.
12. Oregui-Bengoechea, M.; Miletić, N.; Hao, W.; Björnerbäck, F.; Rosnes, M. H.; S. Garitaonandia, J.; Hedin, N.; Arias, P. L.; Barth, T., High-Performance Magnetic Activated Carbon from Solid Waste from Lignin Conversion Processes. 2. Their Use as NiMo Catalyst Supports for Lignin Conversion. *ACS Sustainable Chemistry & Engineering* **2017,** *5* (12), 11226-11237.
13. Thines, K. R.; Abdullah, E. C.; Mubarak, N. M., Effect of process parameters for production of microporous magnetic biochar derived from agriculture waste biomass. *Microporous and Mesoporous Materials* **2017,** *253*, 29-39.
14. Gong, K.; Hu, Q.; Yao, L.; Li, M.; Sun, D.; Shao, Q.; Qiu, B.; Guo, Z., Ultrasonic Pretreated Sludge Derived Stable Magnetic Active Carbon for Cr(VI) Removal from Wastewater. *ACS Sustainable Chemistry & Engineering* **2018,** *6* (6), 7283-7291.
15. Safarik, I.; Horska, K.; Pospiskova, K.; Safarikova, M., Magnetically Responsive Activated Carbons for Bio - and Environmental Applications. *International Review of Chemical Engineering (I.RE.CH.E.)* **2012,** *4* (3).
16. Tsoncheva, T.; Mileva, A.; Tsyntsarski, B.; Paneva, D.; Spassova, I.; Kovacheva, D.; Velinov, N.; Karashanova, D.; Georgieva, B.; Petrov, N., Activated carbon from Bulgarian peach stones as a support of catalysts for methanol decomposition. *Biomass and Bioenergy* **2018,** *109*, 135-146.
17. Pang, Y. L.; Lim, S.; Ong, H. C.; Chong, W. T., Research progress on iron oxide-based magnetic materials: Synthesis techniques and photocatalytic applications. *Ceramics International* **2016,** *42* (1, Part A), 9-34.
18. Zhang, G.; Qu, J.; Liu, H.; Cooper, A. T.; Wu, R., CuFe2O4/activated carbon composite: A novel magnetic adsorbent for the removal of acid orange II and catalytic regeneration. *Chemosphere* **2007,** *68* (6), 1058-1066.
19. Thines, K. R.; Abdullah, E. C.; Mubarak, N. M.; Ruthiraan, M., Synthesis of magnetic biochar from agricultural waste biomass to enhancing route for waste water and polymer application: A review. *Renewable and Sustainable Energy Reviews* **2017,** *67*, 257-276.

20. Yang, N.; Zhu, S.; Zhang, D.; Xu, S., Synthesis and properties of magnetic Fe3O4-activated carbon nanocomposite particles for dye removal. *Materials Letters* **2008,** *62* (4), 645-647.
21. Han, D.; Zhao, Z.; Xu, Z.; Li, Y.; Zhang, P.; Guo, X., β-FeOOH-Coupled Activated Carbon Prepared by the High Temperature Impregnation Method for Bromate Removal from Water. *Journal of Chemical & Engineering Data* **2018,** *63* (6), 2243-2251.
22. Luo, X.; Zhang, L., High effective adsorption of organic dyes on magnetic cellulose beads entrapping activated carbon. *Journal of Hazardous Materials* **2009,** *171* (1), 340-347.
23. Zhang, S.; Tao, L.; Jiang, M.; Gou, G.; Zhou, Z., Single-step synthesis of magnetic activated carbon from peanut shell. *Materials Letters* **2015,** *157*, 281-284.
24. Ruiz, B.; Ferrera-Lorenzo, N.; Fuente, E., Valorisation of lignocellulosic wastes from the candied chestnut industry. Sustainable activated carbons for environmental applications. *Journal of Environmental Chemical Engineering* **2017,** *5* (2), 1504-1515.
25. FAO, **2016**.
26. A.R.E.F.L.H., Livre blanc de la Chataigne Europeenne. **2017**.
27. Assembly of European Regions Producing Fruit, V. a. P. A. R. E. F. L. H.
28. Özçimen, D.; Ersoy-Meriçboyu, A., Removal of copper from aqueous solutions by adsorption onto chestnut shell and grapeseed activated carbons. *Journal of Hazardous Materials* **2009,** *168* (2), 1118-1125.
29. Altıntıg, E.; Onaran, M.; Sarı, A.; Altundag, H.; Tüzen, M., Preparation, characterization and evaluation of bio-based magnetic activated carbon for effective adsorption of malachite green from aqueous solution. *Materials Chemistry and Physics* **2018**.
30. Feiqiang, G.; Xiaolei, L.; Xiaochen, J.; Xingmin, Z.; Chenglong, G.; Zhonghao, R., Characteristics and toxic dye adsorption of magnetic activated carbon prepared from biomass waste by modified one-step synthesis. *Colloids and Surfaces A: Physicochemical and Engineering Aspects* **2018,** *555*, 43-54.
31. Girón, R. P.; Suárez-Ruiz, I.; Ruiz, B.; Fuente, E.; Gil, R. R., Fly Ash from the Combustion of Forest Biomass (Eucalyptus globulus Bark): Composition and Physicochemical Properties. *Energy & Fuels* **2012,** *26* (3), 1540-1556.
32. Altintig, E.; Kirkil, S., Preparation and properties of Ag-coated activated carbon nanocomposites produced from wild chestnut shell by ZnCl2 activation. *Journal of the Taiwan Institute of Chemical Engineers* **2016,** *63*, 180-188.
33. Luo, X.; Lei, X.; Cai, N.; Xie, X.; Xue, Y.; Yu, F., Removal of Heavy Metal Ions from Water by Magnetic Cellulose-Based Beads with Embedded Chemically Modified Magnetite Nanoparticles and Activated Carbon. *ACS Sustainable Chemistry & Engineering* **2016,** *4* (7), 3960-3969.
34. Zuorro, A.; Lavecchia, R.; Natali, S., Magnetically Modified Agro-Industrial Wastes as Efficient and Easily Recoverable Adsorbents for Water Treatment. *Chemical Engineering Transactions* **2014,** *38*.
35. Do, M. H.; Phan, N. H.; Nguyen, T. D.; Pham, T. T. S.; Nguyen, V. K.; Vu, T. T. T.; Nguyen, T. K. P., Activated carbon/Fe3O4 nanoparticle composite: Fabrication, methyl orange removal and regeneration by hydrogen peroxide. *Chemosphere* **2011,** *85* (8), 1269-1276.
36. Pohlmann, J. G.; Osório, E.; Vilela, A. C. F.; Diez, M. A.; Borrego, A. G., Integrating physicochemical information to follow the transformations of biomass upon torrefaction and low-temperature carbonization. *Fuel* **2014,** *131*, 17-27.
37. Chen, B.; Chen, Z.; Lv, S., A novel magnetic biochar efficiently sorbs organic pollutants and phosphate. *Bioresource Technology* **2011,** *102* (2), 716-723.
38. Suppiah, D. D.; Abd Hamid, S. B., One step facile synthesis of ferromagnetic magnetite nanoparticles. *Journal of Magnetism and Magnetic Materials* **2016,** *414*, 204-208.
39. Li, Y.-S.; Church, J. S.; Woodhead, A. L., Infrared and Raman spectroscopic studies on iron oxide magnetic nano-particles and their surface modifications. *Journal of Magnetism and Magnetic Materials* **2012,** *324* (8), 1543-1550.

40. Li, Y.-S.; Church, J. S.; Woodhead, A. L.; Moussa, F., Preparation and characterization of silica coated iron oxide magnetic nano-particles. *Spectrochimica Acta Part A: Molecular and Biomolecular Spectroscopy* **2010,** *76* (5), 484-489.
41. Fu, R.; Wang, W.; Han, R.; Chen, K., Preparation and characterization of γ-Fe2O3/ZnO composite particles. *Materials Letters* **2008,** *62* (25), 4066-4068.
42. Ferrari, A. C.; Robertson, J., Interpretation of Raman spectra of disordered and amorphous carbon. *Phys. Rev. B* **2000,** *61* (20), 14095-14107.
43. Tuinstra, F.; Koenig, J. L., Raman Spectrum of Graphite. *The Journal of Chemical Physics* **1970,** *53* (3), 1126.
44. Rufford, T. E.; Hulicova-Jurcakova, D.; Zhu, Z.; Lu, G. Q., A comparative study of chemical treatment by FeCl3, MgCl2, and ZnCl2 on microstructure, surface chemistry, and double-layercapacitance of carbons from waste biomass. *Journal of Materials Research* **2010,** *25* (8), 1451-1459.
45. Alvear, D.; Galeas, S.; Guerrero, V. H.; Debut, A., Síntesis y Caracterización de Nanopartículas de Magnetita. *Revista Politécnica* **2017,** *39* (2).
46. Jubb, A. M.; Allen, H. C., Vibrational Spectroscopic Characterization of Hematite, Maghemite, and Magnetite Thin Films Produced by Vapor Deposition. *ACS Applied Materials & Interfaces* **2010,** *2* (10), 2804-2812.
47. Murad, E.; Johnston, J. H., Iron Oxides and Oxyhydroxides. *Mössbauer Spectroscopy Applied to Inorganic Chemistry. Gary J. Long, ed., Plenum Press, New York* **1987,** *12*, 507-582.
48. Schaff, P., *Acta Metallurgica et Materialia* **1992,** *40*, 373-379.
49. Thommes, M.; Kaneko, K.; Neimark Alexander, V.; Olivier James, P.; Rodriguez-Reinoso, F.; Rouquerol, J.; Sing Kenneth, S. W., Physisorption of gases, with special reference to the evaluation of surface area and pore size distribution (IUPAC Technical Report). In *Pure and Applied Chemistry*, 2015; Vol. 87, p 1051.
50. Bouremana, A.; Guittoum, A.; Hemmous, M.; Rahal, B.; Sunol, J.J.; Martínez-Blanco, D.; Blanco, J.A.; Gorria, P.; Benrekaa, N., Crystal structure, microstructure and magnetic properties of Ni nanoparticles elaborated by hydrothermal route. *J. Magn. Magn. Mat.* **2014** (358-350) 11-15.
51 Martínez-Blanco, D.;Gorria, P.; Blanco, J.A., Nanostructured Fe obtained by high-energy ball milling. *J. Magn. Magn. Mat.* **2006** (300) e339-e341.